ACS OMEGA

http://pubs.acs.org/journal/acsodf

Article

Light-Assisted Synthesis of Silver and Gold Nanoparticles by New Benzophenone Derivatives

Abrar S. Alnafisah,* Elaf Alqrairy, Haja Tar,* Fahad M Alminderej, Lotfi M. Aroua, Bernadette Graff, and Jacques Lalevee

Cite This: *ACS Omega* 2023, 8, 3207−3220

Read Online

ACCESS | Metrics & More | Article Recommendations | Supporting Information

ABSTRACT: Benzophenone derivatives were evaluated as new photoinitiators in combination with triethylamine (TEA) and iodonium salt (Iod) for very rapid and efficient formation of metal nanoparticles in an organic solvent, by which silver and gold ions were reduced under light at 419 nm (photoreactor) with an irradiation intensity of 250 microwatts/cm^2. The new benzophenone derivatives combined with TEA/Iod salt showed good production of metal nanoparticles (Au^0 and Ag^0) and a small size of nanoparticles of around 4−13 nm. The photochemical mechanisms for the production of initiating radicals were studied using cyclic voltammetry, where a negative ΔG of around −1.96 eV was obtained, which made the process favorable. The obtained results proved the formation of amine and phenyl radicals, which led to the reduction of gold III chloride or silver ions to the gold and silver NPs. The UV−vis spectroscopy technique was used as a very beneficial tool for the surface plasmon resonance band detection of metal nanoparticles. To sum up the results, we have observed that nanoparticles (NPs) were distributed differently in different photoinitiator systems and the particle size also changed by changing the system of initiation. In comparison to the system alone, not only were the nanoparticles smaller but they were also generated within a shorter period of irradiation time for the system BP\Iod\TEA. Finally, the quenching process of benzophenone fluorescence by the gold and silver nanoparticles was investigated.

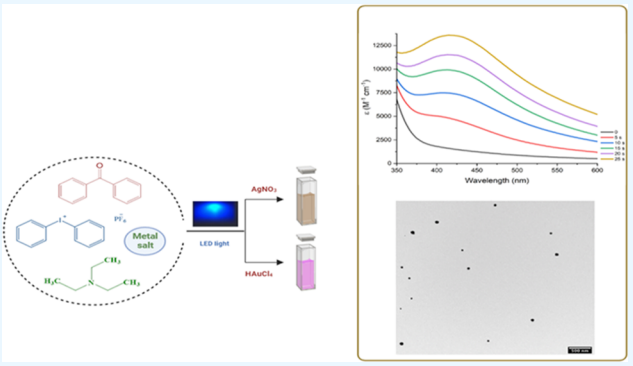

1. INTRODUCTION

Due to their lower reactivity in bulk form, gold and silver have historically been extremely appealing noble metals. The noble metals exhibit specific features and become more reactive when they are combined to create small-sized colloids.[1−3] Noble metals have different optical and absorbance properties depending on their size. Additionally, compared to atoms, surfaces, or macromolecular materials, metal nanoparticles offer excellent characteristics.[4,5] Due to their appropriate elastic light scattering properties, silver nanoparticles (AgNPs) and gold nanoparticles (AuNPs) can be used in optical, imaging, and sensing applications.[6−8] Using the benefits of the metal colloids produced by diverse synthesis techniques is the appropriate course of action because nanostructured metals have many advantages over their molecular state.[9,10] To make metal nanoparticles with various sizes, forms, compositions, and architectures to obtain new capabilities in nanomaterials, several synthetic methods, including physical, chemical, and photochemical methods, have been used.[11−13] Due to a number of benefits, including clean synthesis, fewer by-products, strict irradiation control, lower temperature, simple and inexpensive equipment, less overall energy required to drive the reaction, and spatiotemporal control over the rate of the reaction as well as the degree of reduction,[14−16] the photochemical method was found to be the most preferred method.[17,24] The metal precursor must be reduced by the photocatalyzed action of the reducing agent from its n+ valence state (M$^{(n+)}$) to its zero-valence state (M^0) to start the photochemical reaction.[16] Metallic NPs are created by the M0 form nucleation center or nuclei, which develop and assemble later.[25]

Nanoparticles can be created in a variety of methods. One of these involves the photochemical synthesis of metal nanoparticles via a Norrish type I mechanism involving the intramolecular bond breakage of a photoinitiator in the triplet state to produce two radicals. Since it is a commercial photoinitiator type I, easily accessible, water-soluble, and produces ketyl radicals with a quantum yield of 0.29 in fast photocleavage from a triplet state with a lifetime of just 11 ns,

Received: October 15, 2022
Accepted: December 27, 2022
Published: January 11, 2023

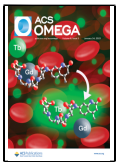

Scheme 1. Chemical Structures of the BP Derivatives Used in This Study: BP1 and BP2

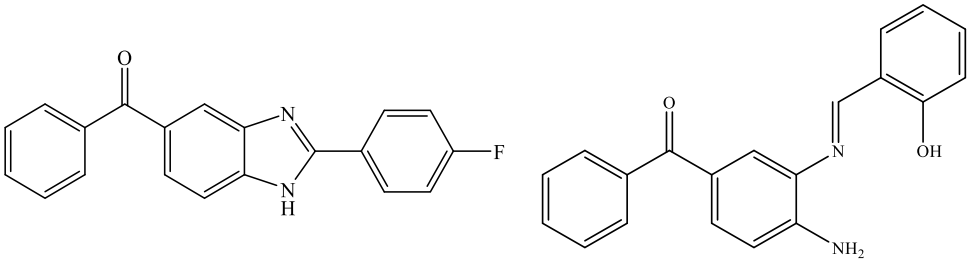

BP1 BP2

Irgacure-2959 (I-2959) has been the most successful photo-releasing reducing agent.[26] Within minutes, stable and unprotected gold nanoparticles were created in an aqueous solution, which photochemically generates 2-hydroxy-2-propyl radicals and lowers Au(III) (as AuCl(−4)) to AuNPs. The impact of radiation on particle size has been researched. The particle size has been found to be smaller and more monodisperse the greater the UVA irradiance and the more uniform the light source.[27] In addition to Au(III), I-2959 also reduces Au(I).[28] Additionally, the creation of AgNPs,[29−31] Au/Ag alloy NPs,[32] Au/Ag core−shell NPs,[33] and CuNPs[34] involved ion reduction by ketyl radicals produced by I−2959 photoinitiators after exposure to UVA. The initial studies described by Itakura et al.[35] used the photoinitiator-type benzoin, in which deaerated ethanol solutions with metal salts [Ag, Au, Cu] and PVP as a stabilizer underwent UVB photolysis to produce both the benzoyl radical and a hydroxybenzyl radical. Additionally, it was used to create AuNPs in the dendrimer PAMAM and expose those particles to UVC radiation for up to 90 min.[36]

In addition to type I mechanisms, type II mechanisms have also been used, in which the radicals were produced via an intermolecular, bimolecular mechanism that is categorized as type II photoinitiation. In this method, hydrogen atoms are extracted from a donor in a single step to produce free radicals. The creation of nanomaterials employing a range of chromophores combined with reactive hydrogen donors for an alternate generation of reducing free radicals has been the focus of research for the past two decades.[37−39] The photoinduced hydrogen atom abstraction by ketones is one of the most significant organic photochemical processes.[40,41] Excited triplet ketones take an atom of hydrogen from a donor and produce two radicals or a biradical in the process. Because they have a low-lying n−π^* state and therefore have a high reactivity for hydrogen abstraction, aryl ketones are frequently used as photochemical sensitizers.[41] Due to its photophysical characteristics, benzophenone is a prime option for producing reducing species for the creation of nanoparticles. For the creation of colloidal nanoparticles, it has been widely employed as a sensitizer.[39,42,43] In one instance, Kapoor et al. synthesized colloidal CuNPs in the presence of CW 253.7 nm light using $CuSO_4$, benzophenone, and poly(vinylpyrrolidone) (PVP) as a stabilizer, where it was investigated how the photosensitizer benzophenone (BP) affected the development of Cu metal particles. They came to the conclusion that the solution did not produce nanoparticles when benzophenone was not present.[44] In a different recent study, CuNPs were created by photoreducing $CuCl_2$ salt in ethanol in the presence of benzophenone, a radical photoinitiator.[45] In the study by Marin et al.,[28] aqueous micellar ketones (benzophenone, xanthone, 1-azaxanthone) in the presence of $HAuCl_4$ resulted in the formation of gold nanoparticles as well. The growth of the particles occurred more quickly in the absence of oxygen than in the presence of oxygen. Studies on the development of nanoparticles with 1,4-cyclohexadiene as hydrogen donors were also carried out. Compared to when the surfactant was the hydrogen donor, the growth of NPs happened much faster (CTAC). The ability of 1,4-cyclohexadiene and 1,3-cyclohexadiene to donate hydrogen to chromophores has also been compared using benzophenone under UVA exposure. When 1,4-cyclohexadiene was used, nanoparticles formed within 5 min, whereas no particles formed within 30 min of exposure time when 1,3-cyclohexadiene was used. Another work showed that AuNPs can be produced photochemically by exploiting the rarely reported nucleophilic property of the benzophenone triplet under the illumination of a 368 nm LED, producing NPs with a spherical form.[46] In further investigations, 4-hydroxybenzophenone was used as a photoreducing agent in an organic solvent for a brief period of time to create AuNPs.[47] Ag^+ is effectively reduced to Ag^0 by ketyl radicals, which are created during the photoreduction of benzophenone.[48,49] With the use of transitory species such as the hydroxy diphenyl methyl radical, Scaiano et al. were able to create silver nanoparticles (NPs) in a matter of minutes.[50]

In this study, an organic solvent was used to photochemically create metal nanoparticles. Iodonium salt and TEA as a hydrogen donor were utilized to speed up the production of ketyl radicals. By employing benzophenone compounds as new photoinitiators, the synthesis can be completed under benign conditions in a matter of minutes as opposed to hours. Additionally, employing various system photoinitiators makes it simple to regulate the particle size.

2. MATERIALS AND METHODS

2.1. Materials. The chemical structures of BP derivatives are presented in Scheme 1. The synthesis and characterization of BP1 were published in the previous study,[51] while the second molecule BP2 is presented in the Supporting Information. The study by Asadi et al. was taken as a reference in the synthesis of BP2.[52] Triethylamine (TEA), silver nitrate ($AgNO_3$, 99.99%), gold (III) chloride hydrate ($HAuCl_4$ 99.99%), methanol, and diphenyl iodonium hexafluorophosphate (Ph_2 I^+) were obtained from Sigma-Aldrich. The structures of some compounds used in this study are given in Scheme 2.

2.2. Irradiation Source. The prepared solution was placed in a Pyrex tube (i.d. 9 mm) and irradiated in a photochemical reactor using a 35 W LED lamp at 419 nm with an irradiation

https://doi.org/10.1021/acsomega.2c06655
ACS Omega 2023, 8, 3207−3220

Scheme 2. Structures of the Other Chemicals Used in This Study: Iodonium Salt (Iod) and Triethylamine (TEA)

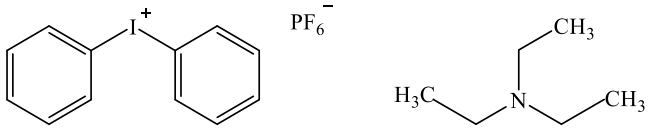

Ph2I+ TEA

intensity of 250 microwatts/cm^2 without a water cooling system in atmospheric air and at room temperature.

2.3. Redox Potentials. The oxidation potentials of photoinitiators BP1 and BP2 (E_{ox} vs SCE) were measured in acetonitrile using cyclic voltammetry with tetrabutylammonium hexafluorophosphate of concentration 0.1 M as a supporting electrolyte. The free energy change ΔG_{et} for an electron transfer reaction was calculated using the classic Rehm−Weller equation (eq 1), in which E_{ox}, E_{red}, E^*, and C stand for the oxidation potential of the electron donor, the reduction potential of the electron acceptor, the excited-state energy level, and the Coulombic term for the initially formed ion pair, respectively.[53] It often occurs that C is neglected in polar solvents, which is the case here.

$$\Delta G_{et} = E_{ox} - E_{red} - E^* + C \quad (1)$$

2.4. Transmission Electron Microscopy (TEM). The morphology and particle size of the metal nanoparticles were examined using a high-resolution transmission electron microscope (HR-TEM, JEOL, JEM-2100, Tokyo, Japan).

2.5. Fluorescence Experiments. The fluorescence properties of the metal nanoparticles were determined in CH_3OH using a JASCO FP-8200 spectrometer (JASCO, Riyadh, Saudi Arabia).

3. RESULTS

3.1. Light Absorption Properties of Benzophenone Photoinitiators. Benzophenones are the most investigated and studied type II photoinitiators.[54] It is known that BP strongly absorbs light within the UV region and presents a $\pi-\pi^*$ transition (with a maximum of 252 nm and an extinction coefficient of around 20 000 mol^{-1} Lcm^{-1}). Moreover, BP exhibits a slight absorption indicating an n$-\pi^*$ in the range of 350 nm with ε = 100 mol^{-1} Lcm^{-1} as a shoulder of the $\pi-\pi^*$ transitions.[55,56] The absorption characteristics of the photoinitiators BP1 and BP2 in this study were compared with BP as the model compound in this study (Figure 1 and Table 1). The

Table 1. Values of λ_{max} and ε_{max} of Benzophenone and Its Derivatives (BP1, BP2) in Methanol

BP	ε (M^{-1} cm^{-1})	λ_{max} (nm)
BP	20 000	252
BP1	10 437	292
BP2	13 914	294

ground state of the new photoinitiators in a methanol-significant red shift of the $\pi-\pi^*$ transitions (292 and 294 nm) was observed due to the electron-donating effect of fluorine, nitrogen, and oxygen, directly attached to the BP unit.[57] The n$-\pi^*$ transitions of BP1 and BP2 are shifted to 370 nm with a higher extinction coefficient of around 17 500 mol^{-1} Lcm^{-1} compared to the benzophenone parent.

The UV−vis absorption spectra of BP1 and BP2 were predicted using TDDFT calculations (UB3LYP/6−31G* level) (as in Figure 2). A bathochromic shift is observed for BP2 vs BP1, which confirms the experimental finding (seen in Figure 1). The $\pi-\pi^*$ transitions were observed between the frontier orbitals (highest occupied molecular orbital "HOMO" and lowest unoccupied molecular orbital "LUMO"). Additionally, partial charge transfer transitions were observed in which the HOMO and LUMO were delocalized in marginally different positions.

The red shift of BP1 and BP2 versus benzophenone is due to the enhanced π electron delocalization in the molecule as well as the charge transfer of the HOMO to LUMO transition revealed through MO calculations (seen in Figure 2).

To examine the photolysis of the photoinitiators, the evolution of UV−vis spectra of their solution recorded in

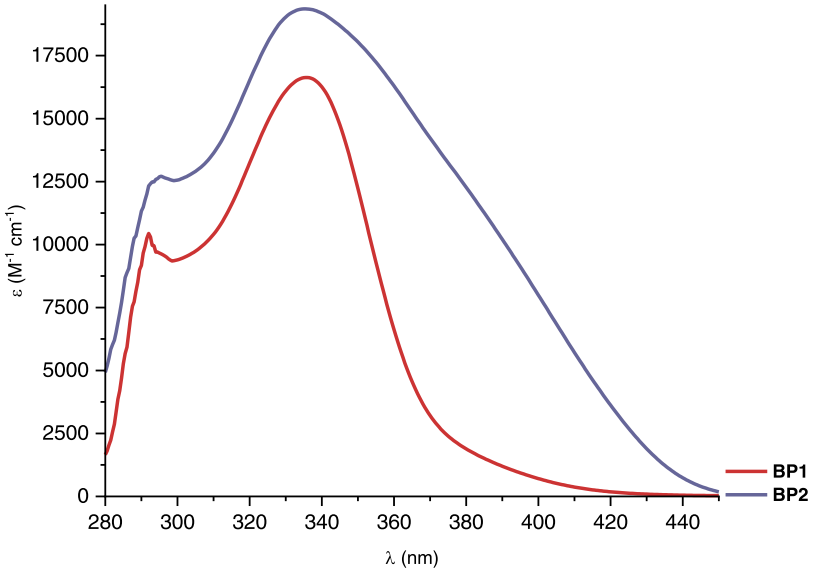

Figure 1. UV−vis absorption spectra of the observed benzophenone derivatives BP1 and BP2 (10^{-4} M) in methanol.

https://doi.org/10.1021/acsomega.2c06655
ACS Omega 2023, 8, 3207−3220

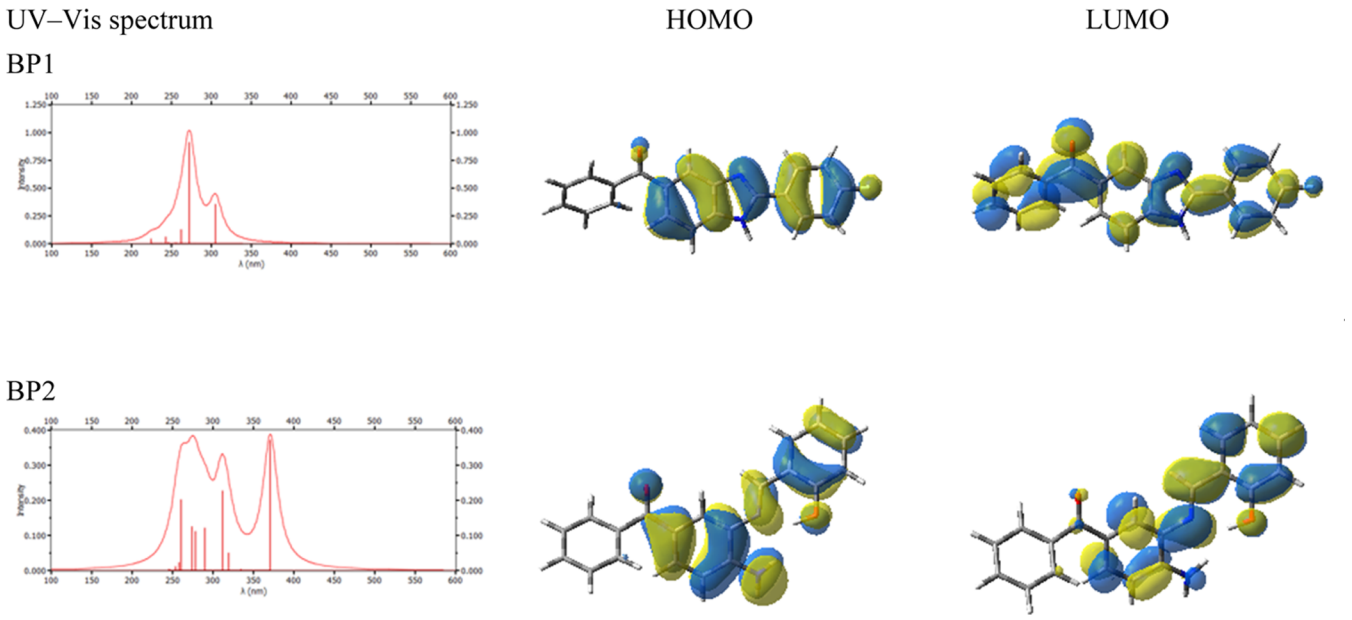

Figure 2. Frontier orbitals HOMO and LUMO in addition to the predicted spectra of the BPs derivatives BP1 and BP2.

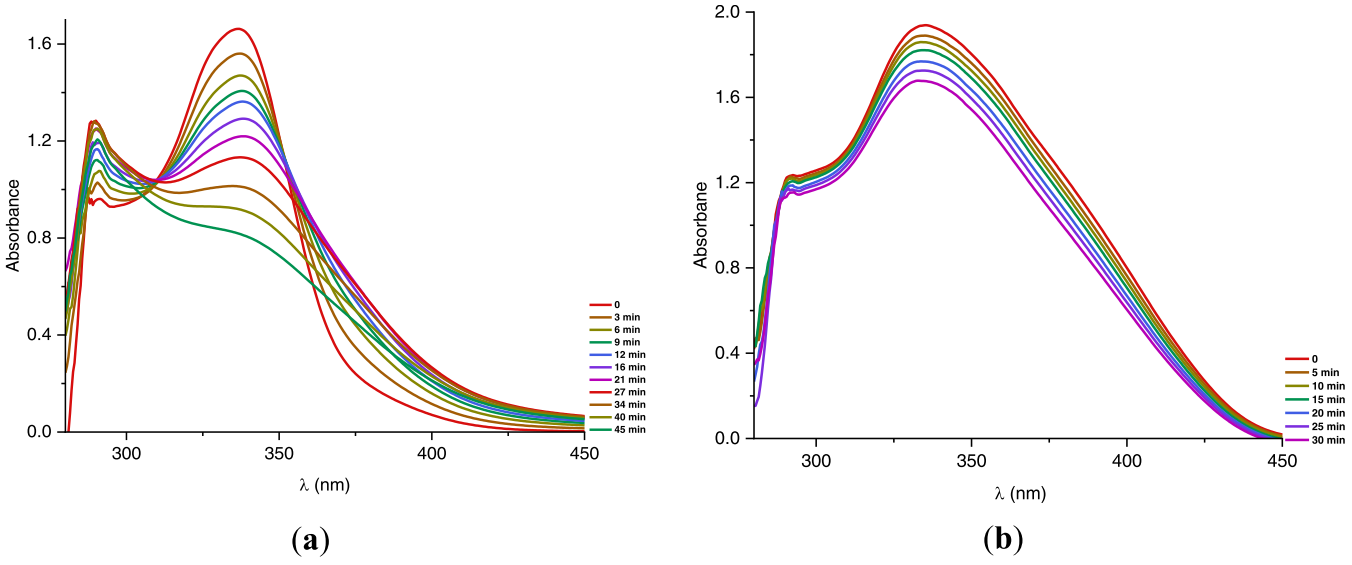

Figure 3. Steady-state photolysis of (a) BP1 and (b) BP2 concentrations of 10^{-4} M using the LED lamp at 419 nm with an irradiation intensity of 250 microwatts/cm^2; UV−vis spectra were recorded at different irradiation times.

Table 2. Excited-State Energies E^*, Oxidation Potentials E_{ox}, and Free Energy Change (ΔG_{et}) for the PBs/Iod/TEA Interaction

PIs	E_{ox} [V]	E_{red} [V]	E^* [eV]	ΔG_{et} (BP/Iod) (eV)	ΔG_{et} (BP /TEA) (eV)
BP1	1.44	−0.48	3.52	−1.88	−1.96
BP2	1.33	−0.41	3.1	−1.57	−1.61

methanol was conducted under 419 nm light irradiation with different exposure times. Figure 3 shows the decrease in the absorbance at 337 and 334.5 nm for BP1 and BP2, respectively. A possible cause for the decrease in the absorbance of BP1 at 337 nm is the hydrogen abstraction of the benzophenone carbonyl group from the solvent.[57] When the irradiation period was increased to 45 min, a rapid decrease in absorbance at 337 nm was observed to the point of almost disappearing. Under the same conditions, the decrease in the absorption of BP2 occurred gradually throughout 30 min of irradiation, which could be ascribed to the very low concentration of BP2 in methanol impeding the bimolecular interactions.[58] [Figure 3b].

3.2. Photoinitiator Oxidation Process. The oxidation potentials E_{ox} of the photoinitiators BP1 and BP2 in acetonitrile are presented in Table 2. This oxidation potential was evaluated by measuring cyclic voltammetry with 0.1 M tetrabutylammonium hexafluorophosphate as a supporting electrolyte. Bubbling nitrogen gas was used to remove the dissolved oxygen (see Figure S3). The excited-state energies

https://doi.org/10.1021/acsomega.2c06655
ACS Omega 2023, 8, 3207−3220

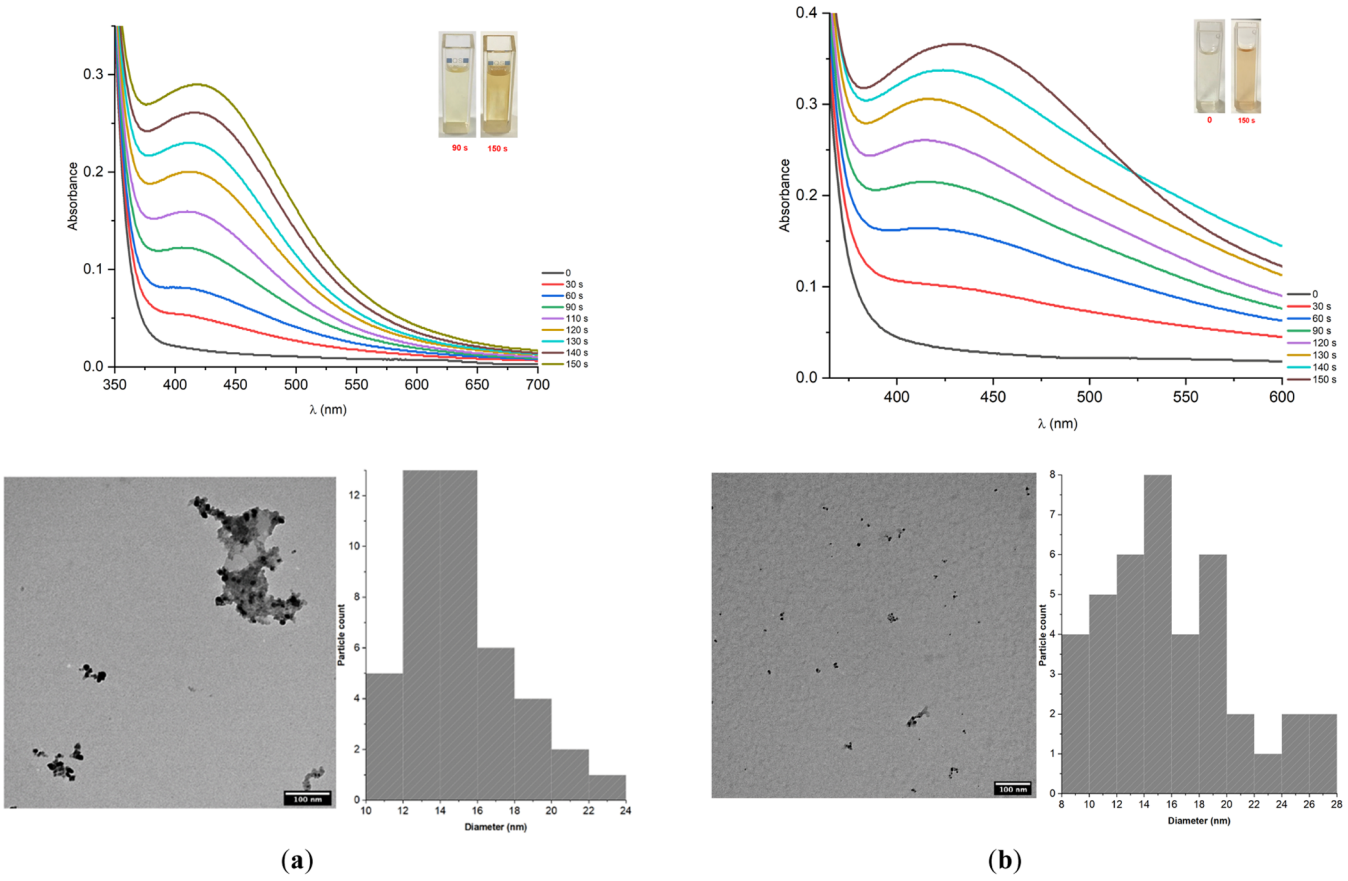

Figure 4. UV−vis absorption spectrum of AgNPs obtained from photoreduction of $AgNO_3$ [2 wt %] with (a) BP1 [0.003 wt %], (b) BP2 [0.003 wt %], and $AgNO_3$ [2 wt %] in CH_3OH depending on the irradiation time (LED 419 with 250 mW/cm^2). Corresponding TEM images of AgNPs with their respective size distributions.

were evaluated from the crossing point of the absorption and luminescence spectra (see Figure S4).

The free energy change ΔG_{et} for the electron transfer reaction between the photoinitiator BP and diphenyl iodonium hexafluorophosphate (Iod), TEA, or gold chloride was calculated using the classical Rehm−Weller equation (eq 1).[59] The values of the free energy change (ΔG_{et}) were found as follows: BP1/Iod: $\Delta\Delta G_{et}$ = −1.88 EV, BP2/Iod: = −1.57 (using E_{red} (Iod) = −0.2 eV).[60] These results are highly negative, which makes the process favorable. The counter-anions of the iodonium salts would not affect the results of the photochemical mechanism study for the initiation process. In addition, the free energy changes (ΔG_{et}) for the electron transfer reaction between PIs (as electron acceptors) and TEA (as electron donors) were obtained as follows: BP1/TEA: ΔG_{et} = −1.96 eV, BP2/TEA: =−1.61 eV (using E_{ox} = 1.079 V for triethylamine).[61] This also supports a favorable electron transfer.

3.3. Photoinduced Synthesis of Metal NPs with a Benzophenone Derivative in Methanol Solution. The nanoparticles of silver and gold display a strong and harmonized oscillation of surface electrons in their conduction band. This induces a strong absorption of their resonant frequencies in the visible area of the electromagnetic spectrum. The absorbance red-shifts to lower energies when the distance between the particles increases or decreases. The silver nanoparticles, then, seem brown and yellow, while the gold nanoparticles illustrate purple and blue tones.[18−23] A metal's Surface plasmon resonance "SPR" band can be defined as these distinguishing plasmon resonance absorbances.[62,63] The frequency of oscillations depends on the metal, the particle size and shape, the interparticle distance, temperature, dielectric constant, and viscosity of the medium.[64] Noble metals demonstrate an intense resonance because of the strong coupling between the plasmon transition and interband excitation. The higher polarizability of mobile conduction band electrons is also a reason for that.[8,65]

3.3.1. AgNPs in Methanol. The radicals formed from the photoreduction of benzophenone (BP1 and BP2) in the presence of a hydrogen donor can generate silver nanoparticles in solutions. The surface plasmon resonance band is observed at around 390−450 nm under exposure to an LED at 419 nm and an intensity of 250 mW/cm^2. Here, iodonium (Iod) salt was utilized and triethylamine (TEA), which is a brilliant hydrogen donor, was used to encourage the production of amine and phenyl radicals.

In Figure 4a, we can see the UV−vis absorption spectra for BP1 0.003 wt % and $AgNO_3$ 2 wt % when irradiated with an LED @419 nm. Therefore, the examination of the spectral changes of the irradiated solution showed that the intensity of the absorbance of BP at 350 nm reduced with time, harmoniously with the emergence of an intense absorption band at about 412 nm (after 60 s of irradiation) because of the surface plasmon resonance, which is characteristic to the AgNPs. Furthermore, one can note that the latter intensity amplified and red-shifted so that, after 150 s of irradiation, the absorption maximum can be recognized at 422 nm (see Figure 4). It concurs that the concentration of AgNPs is amplified

https://doi.org/10.1021/acsomega.2c06655
ACS Omega 2023, 8, 3207−3220

probably because of the breakdown of the nanoparticles into smaller sizes. The TEM analysis substantiates the small size of nanoparticles. The silver nanoparticles' size is small, almost spherical, and varies between 8 and 28 nm for BP2\Ag and 10−24 nm for BP1/Ag. Conversely, the yellow color detected during the irradiation time of the systems verifies the existence of nanometric silver particles with varying sizes.[66] Taking into account the mechanism of photoreduction, the chronological steps preceding the decrease of Ag^+ are demonstrated in Scheme 3. The effect of ketyl radicals on the effective reduction of ions into metal nanoparticles is known.[28,67]

Scheme 3. Reduction of Silver Ions by the Ketyl Radical

$$BP + light \longrightarrow BP^* \quad (1)$$

$$BP\text{-}H^{\bullet} + Ag^+ \longrightarrow BP + H^+ + AgNPs \quad (2)$$

In the second method for the photoinduced creation of silver nanoparticles, samples comprising 0.003% BP derivatives, 1% TEA, and 2 wt % of $AgNO_3$ in 10 mL of methanol were concocted in a quartz cuvette. The role of the hydrogen donor in the materialization of the ketyl radical from benzophenone is taken up by TEA. The Ag^+ reduction was noticed through the shape of the plasmon resonance accompanied with Ag^0 particles that matured in the visible range (Figure 5) after a 25-s exposure. The maximum absorption intensity in the case of BP2 is weak and broad compared with BP1 (Figure 5). Figure 5 demonstrates the absorption spectra of the surveyed systems based on BP1 or BP2 (0.003 wt %) in the existence of silver nitrate (2 wt %) and triethylamine (1 wt %). For the sample containing BP1, the band was primarily located at 413 nm when the irradiation was 5 s. It went through a radical red shift as the irradiation was amplified (i.e., to 416 and 420 nm when exposed to 10 and 25 s, respectively). Considering the sample containing BP2, the max absorbance of the SPR band red-shifted to a longer wavelength with a growing irradiation time from 5 to 25 s at 425 to 432 nm, respectively. The absorption at 432 nm was recognized as an outcome of the presence of small spheroidal AgNPs in solution.[68,69]

It is worth noting that the samples with TEA presented a considerable increase in plasmon band formation put side by side with samples without it. Moreover, the plasmon bands of silver nanoparticles produced in the presence of TEA were all more symmetrical. The TEM images display a small size and spherical shape with a mean fine diameter of silver nanoparticles (4−14 and 8−18 nm) compared to the one component system (see Figure 5). The photoreduction mechanism of $AgNO_3$ to AgNPs is portrayed in Scheme 4. The interaction of the excited state of BP with TEA as a possible hydrogen donor gave rise to the formation of both, the ketyl radical and the amine radical.

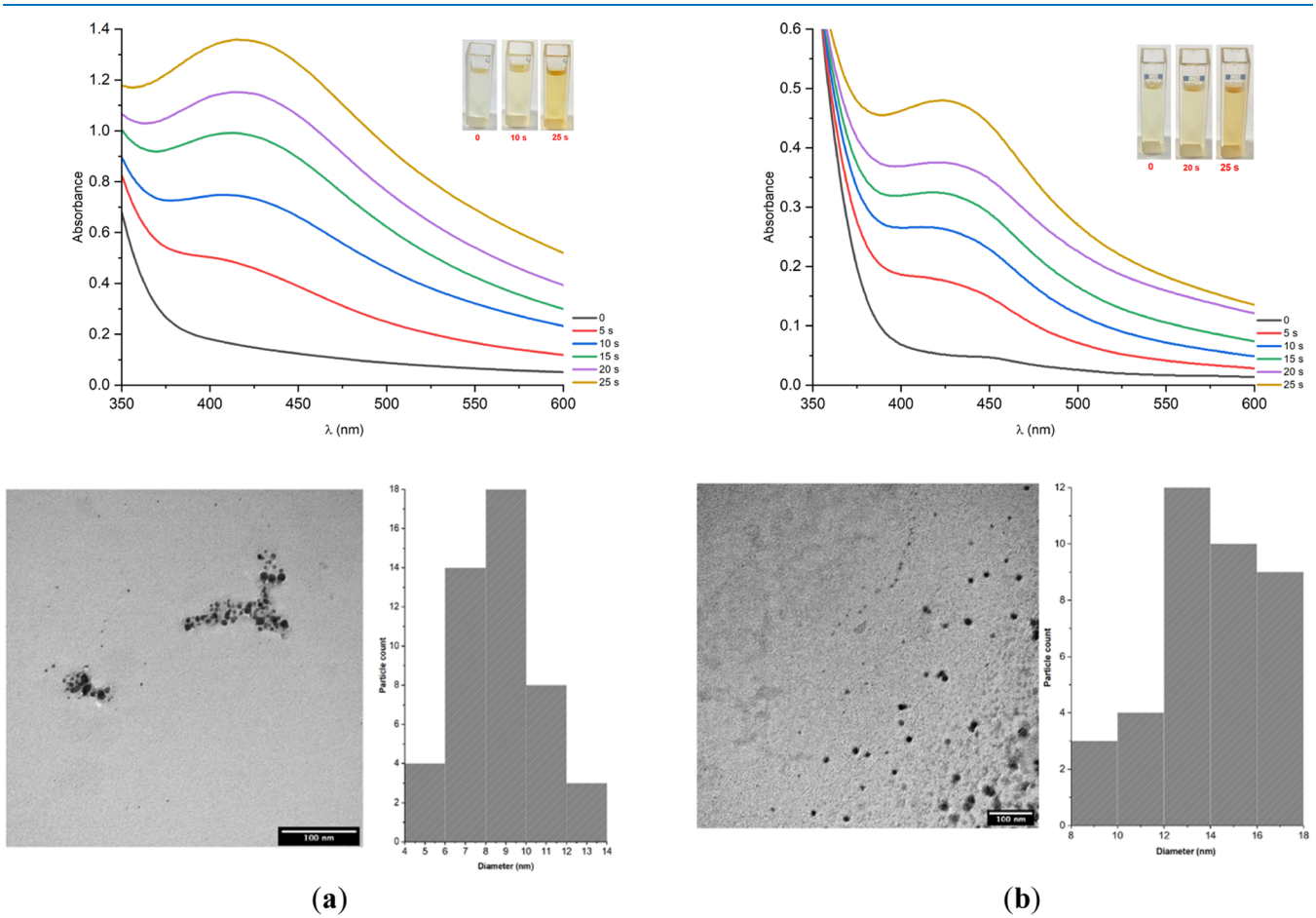

Figure 5. Evolution of the absorption spectra of irradiated mixtures (λ_{irr} = 419 nm, irradiation intensity of 250 microwatts/cm^2). Solution: (a) BP1 0.003 wt %, $AgNO_3$ 2 wt %, and TEA 1 wt %. (b) BP2 0.003 wt %, $AgNO_3$ 2 wt %, and TEA 1 wt % dissolved in 10 mL of methanol. Corresponding TEM images of AgNPs with their respective size distributions.

https://doi.org/10.1021/acsomega.2c06655
ACS Omega 2023, 8, 3207−3220

Scheme 4. Photochemical Synthesis of Colloidal AgNPs by BP1−2 Based on the BP/TEA/$AgNO_3$ System

$BP^* + amine \longrightarrow BP\text{-}H^{\bullet} + Ag^+ \longrightarrow AgNPs$ (1)

$BP^* + amine \longrightarrow amine^{\bullet} + Ag^+ \longrightarrow AgNPs$ (2)

The UV−visible spectra of samples comprising benzophenone 1−2 0.003%, TEA 1%, $AgNO_3$ 2%, and Iod salt 1 wt % are displayed in Figure 6. The plasmon band intensity showed a radical increase of around 400−450 nm when the samples are irradiated for 15 s. As for the sample comprising the BP1, the absorption spectra of the SPR red-shifted from 420 to 428 nm, i.e., from yellow to dark brown with an increase in the irradiation time. This observation is proof of the size increase in silver nanoparticles. The same trend was also observed for the other sample BP2, but it happened at shorter wavelengths compared to the BP1, and the absorption spectra of this sample were linked with small (3−20 nm) spherical metal nanoparticles. In general, the shorter the wavelength of the SPR, the smaller the nanoparticles.[70] The description by TEM confirms the nanoscale size of the silver particles. The sample acquired with BP1 specifies the development of spherical nanoparticles with diameters in the 2−14 nm region. In the case of BP2, the TEM analysis of the sample designates also the development of spherical nanoparticles with diameters between 4 and 9 nm. When compared to earlier systems, these sizes are tremendously small. The projected reaction mechanism of synthesis of AgNPs from BP/TEA/Iod/$AgNO_3$ is presented in Scheme 5.

Scheme 5. Photochemical Synthesis of Colloidal AgNPs with BP1−2 Based on the BP/Iod/TEA/$AgNO_3$ System

$BP + light \longrightarrow BP^*$ (excited state) r1

$BP^* + Ar_2I^+ \longrightarrow BP^+ + Ar^{\bullet} + ArI$ r2

$BP^* + amine \longrightarrow BP^- + amine^{\bullet +}$ r3

$amine^{\bullet +} \longrightarrow amine^{\bullet} + H^+$ r4

$BP^* + Ag^{+1} \longrightarrow BP^+ + Ag^0$ r5

$amine^{\bullet} + Ag^{+1} \longrightarrow amine^{+} + Ag^0$ r6

3.3.2. AuNPs in Methanol. Gold nanoparticles are produced using the same procedure through which silver nanoparticles are produced. The absorption spectra of the samples were measured and recorded as shown in Figure 7 under irradiation of 419 nm and an intensity of 250 mW/cm^2 for a period of 20 min. The BP1 0.003 wt % and gold III chloride 4 wt % resulted in a broad surface plasmon band of low intensity at 555 nm. For that, increasing the irradiation time was noticed to result in

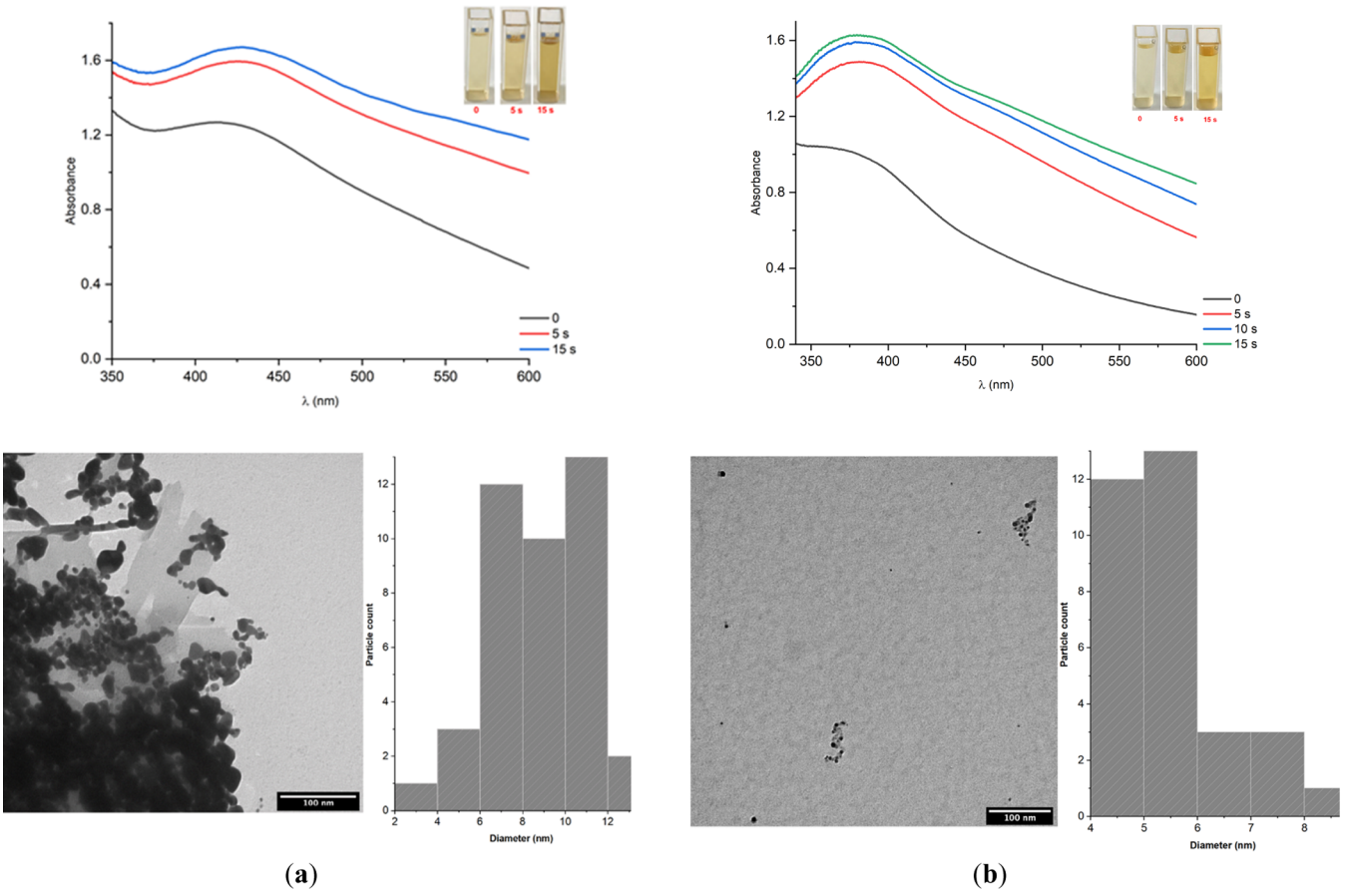

Figure 6. Evolution of the absorption spectra of irradiated mixtures (λ_{irr} = 419 nm, irradiation intensity of 250 microwatts/cm^2). Solution: (a) BP1 0.003 wt %, $AgNO_3$ 2 wt %, TEA 1 wt %, and iodonium salt 1 wt %. (b) BP2 0.003 wt %, $AgNO_3$ 2 wt %, TEA 1 wt %, and iodonium salt 1 wt % dissolved in 10 mL of methanol. Corresponding TEM images of AgNPs with their respective size distributions.

https://doi.org/10.1021/acsomega.2c06655
ACS Omega 2023, 8, 3207−3220

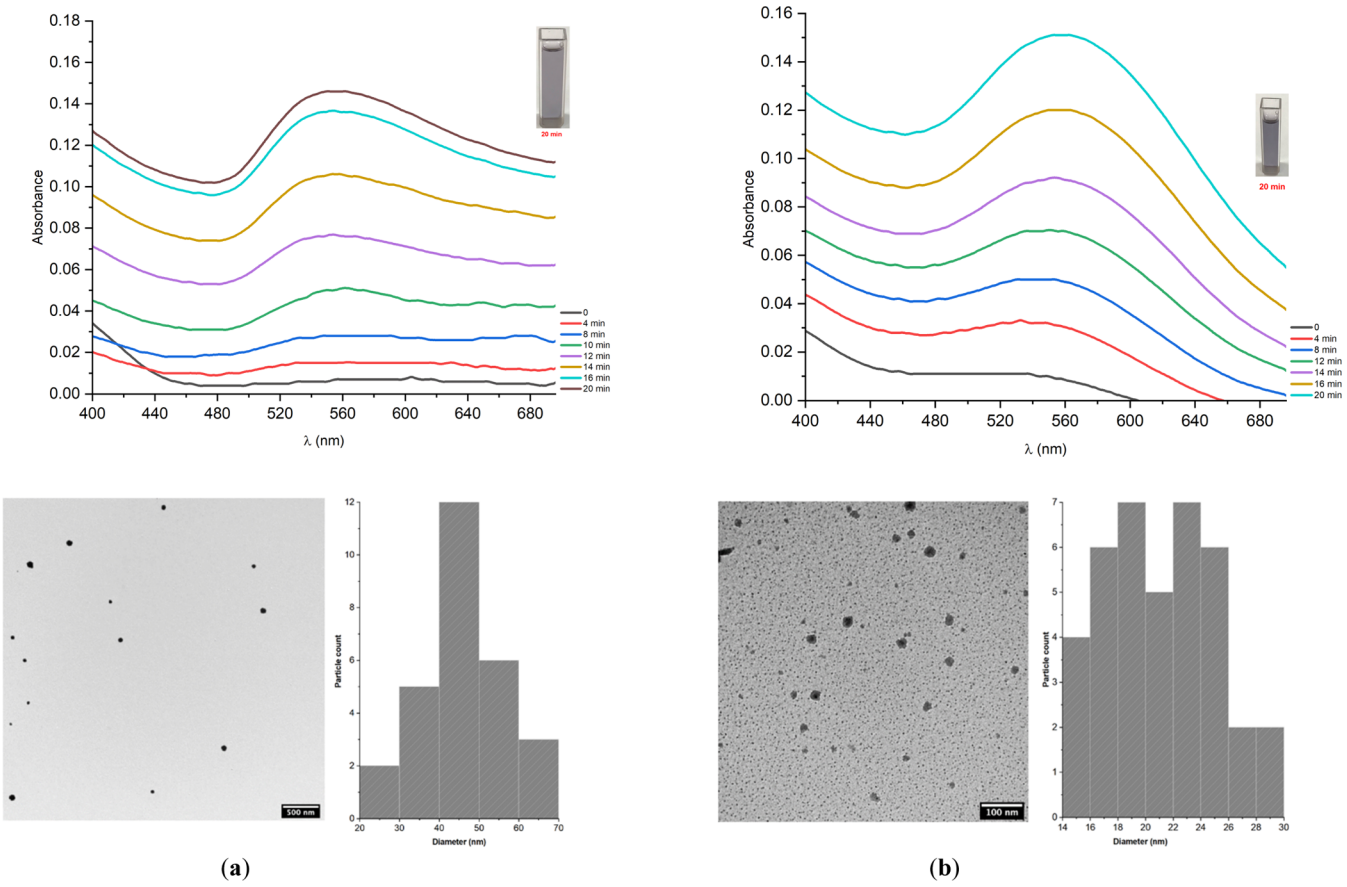

Figure 7. Illustration of the absorption spectrum of gold nanoparticles obtained from photoreduction of $HAuCl_4$ [4 wt %] with (a) BP1 [0.003 wt %] and (b) BP2 [0.003 wt %] in CH_3OH depending on the irradiation time by UV−vis spectroscopy and corresponding TEM images of AuNPs with their respective size distributions.

a red shift, which suggests smaller and more monodisperse nanoparticles as shown in Figure 7a.[27] The absorption spectra of the sample containing BP2 0.003 wt % and gold III chloride 4 wt % after 8 min of irradiation at 553 nm are noticed to present an absorption band in the visible range, which corresponds to the SPR of gold nanoparticles of diameters less than 50 nm (Figure 7b).[71,72]

The TEM images show the nanoparticles produced by the species generated from the photolysis of BP, which exhibit a multimodal size, whereas BP2 generates gold nanoparticles in small sizes. These indicate the formation of spherical nanoparticles with diameters between 14 and 30 nm, while the BP1 compound resulted in spherical nanoparticles of diameters between 20 and 70 nm. The particles were homogeneous in size with no observable agglomeration. The photoreduction of gold nanoparticles is shown in Scheme 6 following a series of reduction and disproportionation. Au^{+3} is reduced to Au^{+2}. However, its instability causes a fast disproportionation. Moreover, in the presence of another ketyl radical, Au^{+1} is reduced to Au^0.

Scheme 6. Photochemical Synthesis of Colloidal AuNPs with BP1−2 Based on the BP/$HAuCl_4$ System

$$BP\ (light) \longrightarrow BP^* \longrightarrow BP\text{-}H^{\bullet} \quad (1)$$

$$BP\text{-}H^{\bullet} + Au^{+3} \longrightarrow Au^{+2} \longrightarrow Au^{+1} \longrightarrow AuNPs \quad (2)$$

The formation of gold nanoparticles utilizing benzophenone as a photoreducer was investigated in the presence of TEA as a hydrogen donor in methanol solutions. When the α-hydrogen is the species abstracted, amines are most likely to be reactive hydrogen donors. The mechanism for ketyl radical formation is explained as follows: it occurs through reactive electron transfer, which forms the ketyl radical anion and amino radical cation. The rapid growth of nanoparticles via TEA can be ascribed to how easy the hydrogen abstraction is. The mechanism is illustrated in Scheme 7. The change in

Scheme 7. Photochemical Synthesis of Colloidal AuNPs with BP1−2 Based on the BP/TEA/ $HAuCl_4$ System

$$BP^* + amine \longrightarrow BP\text{-}H^{\bullet} + Au^{+3} \longrightarrow AuNPs \quad (1)$$

$$BP^* + amine \longrightarrow amine^{\bullet} + Au^{+3} \longrightarrow AuNPs \quad (2)$$

absorption at different irradiation periods is shown in Figure 8. The solution was noted to be very clear and pale purple for approximately 5 s, before turning dark purple after an extended irradiation period of 25 s. As suggested in Figure 8, the SPR development was very fast, reaching a maximum after 25 s and then becoming stable. At the same time, the SPR maximum of BP1 slightly red-shifts from 550 to 570 nm, whereas BP2 exhibits similar behavior as in BP1, with only a slight increase in the gold band observed. Its maximum absorption wavelength underwent a red shift to 575 nm. Using transmission electron microscopy analysis on the samples above, the

https://doi.org/10.1021/acsomega.2c06655
ACS Omega 2023, 8, 3207−3220

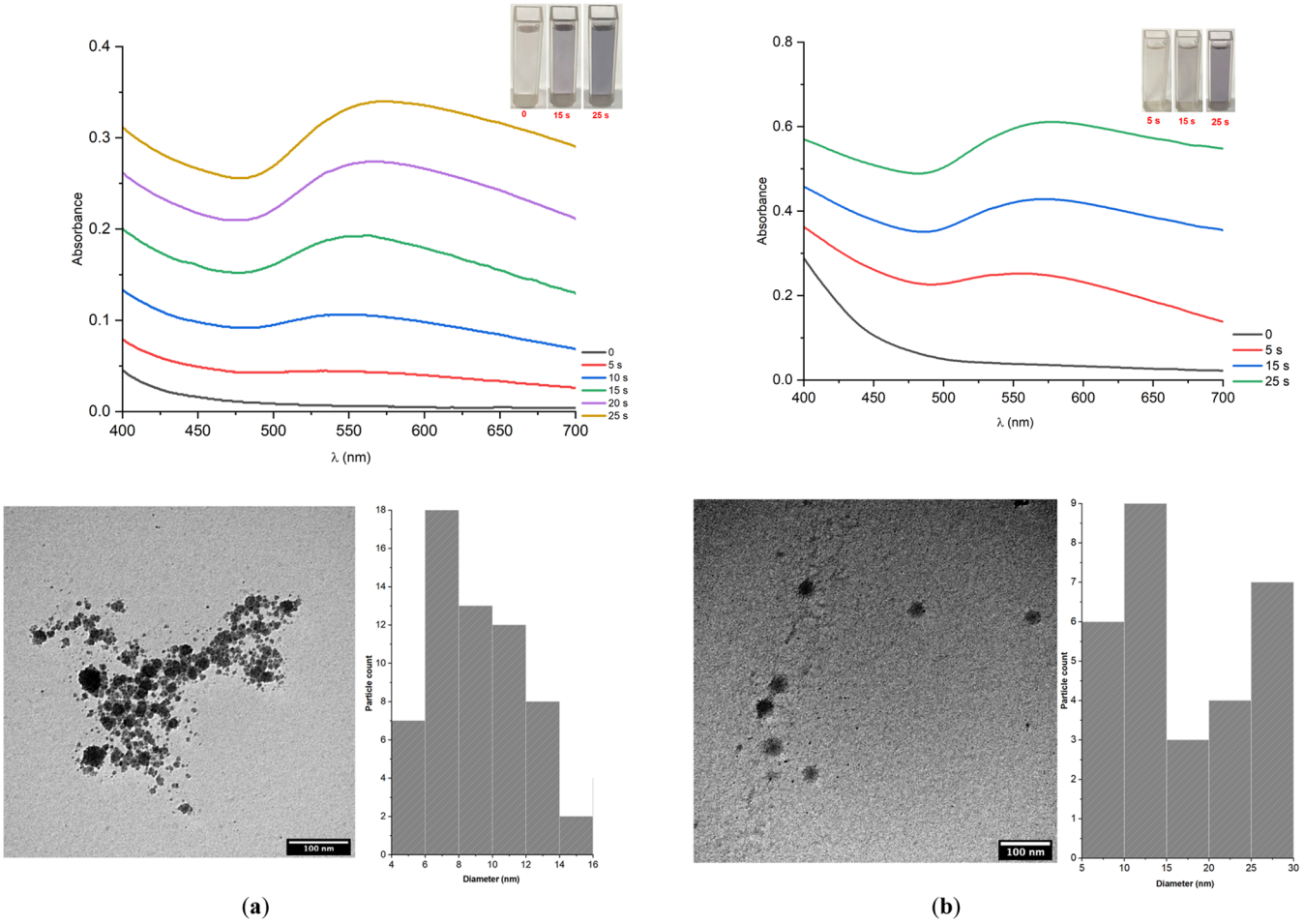

Figure 8. Evolution of the absorption spectra of irradiated mixtures (λ_{irr} = 419 nm, irradiation intensity of 250 microwatts/cm^2). Solution: (a) BP1 0.003 wt %, $HAuCl_4$ 4 wt %, and TEA 1 wt %. (b) BP2 0.003 wt %, $HAuCl_4$ 4 wt %, and TEA 1 wt % dissolved in 10 mL of methanol. In addition to the corresponding TEM images of AuNPs with their respective size distributions.

formation of spherical particles with diameters of 4−16 nm for BP1 and 5−30 nm for BP2 was observed.

The time evolution of the UV−vis spectra of the samples that were synthesized with the hydrogen donor TEA and iodonium salt in BP1 and BP2 is shown in Figure 9. The color of the samples was noticed at different exposure periods to follow the progress of the reaction during the irradiation (in Figure 9). The changes in UV−vis spectra can be said to be related to the formation of AuNPs and the adjustment in their size and shape. Figure 9 illustrates a slight shift in λ_{max} (<5 nm) toward longer wavelengths that is observed in this system. The λ_{max} of BP1 shifts with the irradiation period from 565 nm after 5 s to 570 nm after 15 s. However, in BP2, these values are 545 and 550 nm, respectively. Additionally, the plasmon bands generated from BP1 were observed to be of longer wavelengths than those generated from BP2. After a detailed inspection of the TEM images of the particles generated by BP\TEA\Iod \Au, the presence of smaller particles (4−16 nm) compared to the first system was noted. Interestingly, all of these structural observations can be attributed to the development and subsequent evolution of the corresponding surface plasmon bands during irradiation. Scheme 8 depicts the photoreduction mechanisms for BP/Iod/TEA/Au in the methanol solution.

To summarize, we can say whether BP1 and BP2 had photoinitiator and photoreduction agent roles that supported the possibility to formulate both silver and gold nanoparticles in methanol solutions in a significantly shorter time and with very refined size control. Among the tested systems, the third one can generate AgNPs and AuNPs in shorter irradiation periods compared to the other systems. The position of the SPR maxima and the growth periods for the various systems can be found in Table 3.

3.4. Fluorescence Studies. Fluorescence quenching of the probes by AuNPs and AgNPs has been well explored in the fundamental studies of nanoscale physics alongside their various applications.[73] Fluorescence quenching refers to the process that decreases the fluorescence intensity of a molecule, which is achieved through various molecular interactions including excited-state reactions, energy transfer, molecular rearrangements, collisional quenching, and ground-state complex formation.[74] Quenching can be classified according to the nature of the interaction into static or dynamic. In static quenching, a complex is formed between the fluorophore and quencher in the ground state that is nonfluorescent, whereas collision-based dynamic quenching is characterized by diffusive encounters between the fluorophore and the quencher within the lifetime of the excited state. Owing to their high molar extinction coefficients and tunable absorption spectra in the visible range, nanoparticles are superb quenchers. The initial works of Dulkeith et al. discussed the major fluorescence quenching of the lissamine dye molecules chemically attached to AuNPs of different sizes.[75]

https://doi.org/10.1021/acsomega.2c06655
ACS Omega 2023, 8, 3207−3220

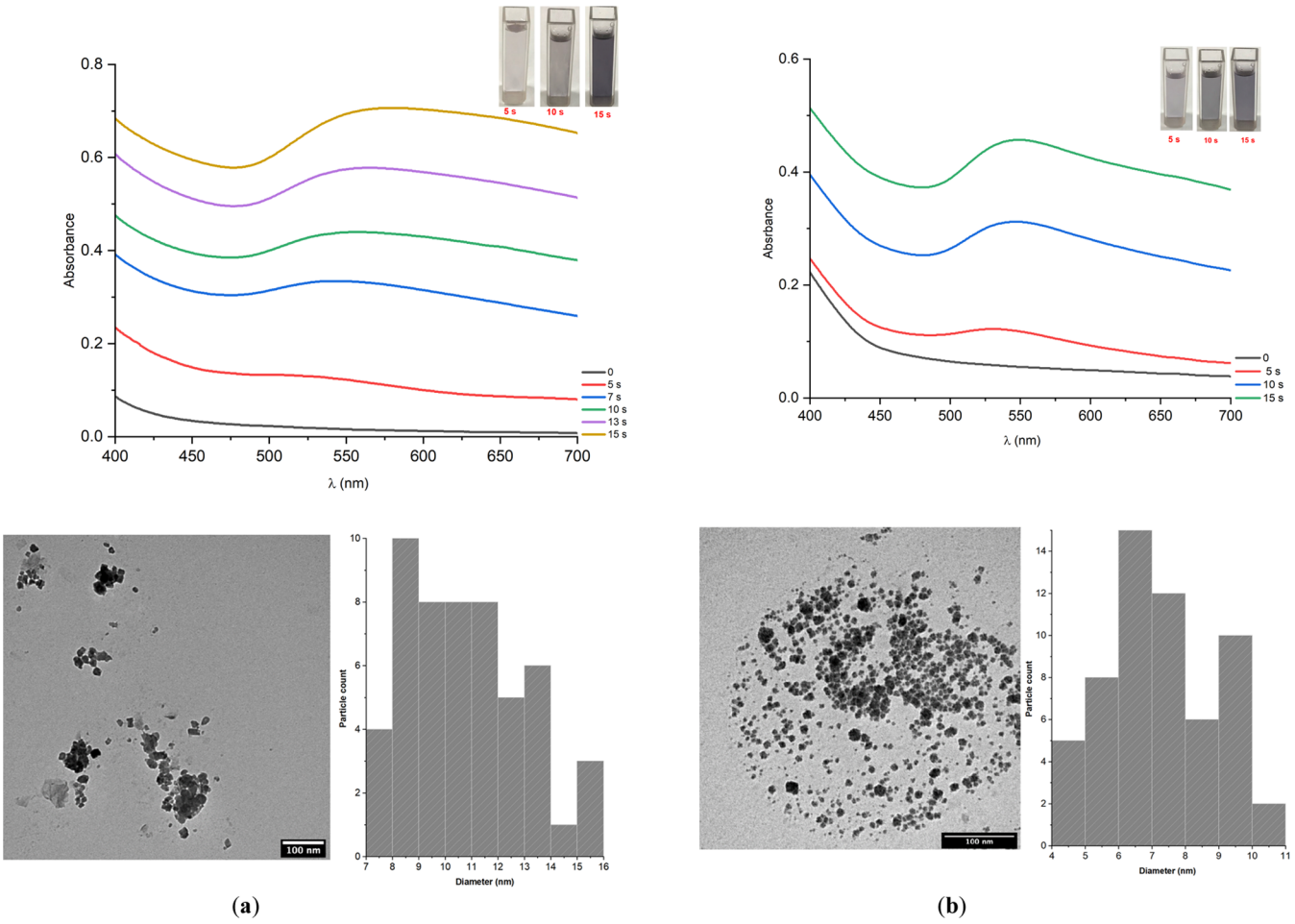

Figure 9. Evolution of the absorption spectra of irradiated mixtures (λ_{irr} = 419 nm with an irradiation intensity of 250 microwatts/cm^2). Solution: (a) BP1 0.003 wt %, $HAuCl_4$ 4 wt %, TEA 1 wt %, and iodonium salt 1 wt %. (b) BP2 0.003 wt %, $HAuCl_4$ 4 wt %, TEA 1 wt %, and iodonium salt 1 wt % dissolved in methanol. This is in addition to the corresponding TEM images of AuNPs with their respective size distributions.

Scheme 8. Photochemical Synthesis of Colloidal AuNPs with BP1−2 Based on the BP/Iod/TEA/$HAuCl_4$ System

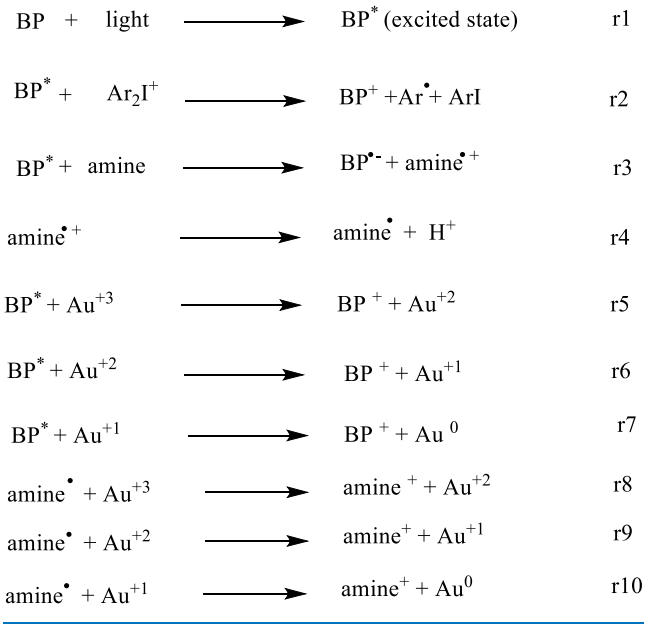

Figure 10 displays the fluorescence spectra of BP-AgNPs and BP-AuNPs in the presence and absence of TEA and Iod salt.

Table 3. Summary of the Spectral Data and Signal Growth Information for (a) Silver Nanoparticles and (b) Gold Nanoparticles Produced from BP Derivatives in the Various Studied Systems

(a) AgNPs						
	BP/Ag		BP/Ag/TEA		BP/Ag/-TEA/Iod	
systems	BP1	BP2	BP1	BP2	BP1	BP2
growth time	150 s		25 s		15 s	
SPR maximum (nm)	422	435	420	435	428	385
size (nm)	10−24	8−28	4−14	8−18	2−14	4−9
(b) AuNPs						
	BP/Au		BP/Au/TEA		BP/Au/-TEA/Iod	
systems	BP1	BP2	BP1	BP2	BP1	BP2
growth time	20 min		25 s		15 s	
SPR maximum (nm)	555	553	570	575	570	550
size	20−70	14−30	4−16	5−30	7−16	4−11

These spectra were measured with average diameters of 6−40 nm (as determined by TEM shown in Figures 6 and 9 for TEM micrographs) with an excitation wavelength of 350 nm. It was observed that the fluorescence intensity increases with

https://doi.org/10.1021/acsomega.2c06655
ACS Omega 2023, 8, 3207−3220

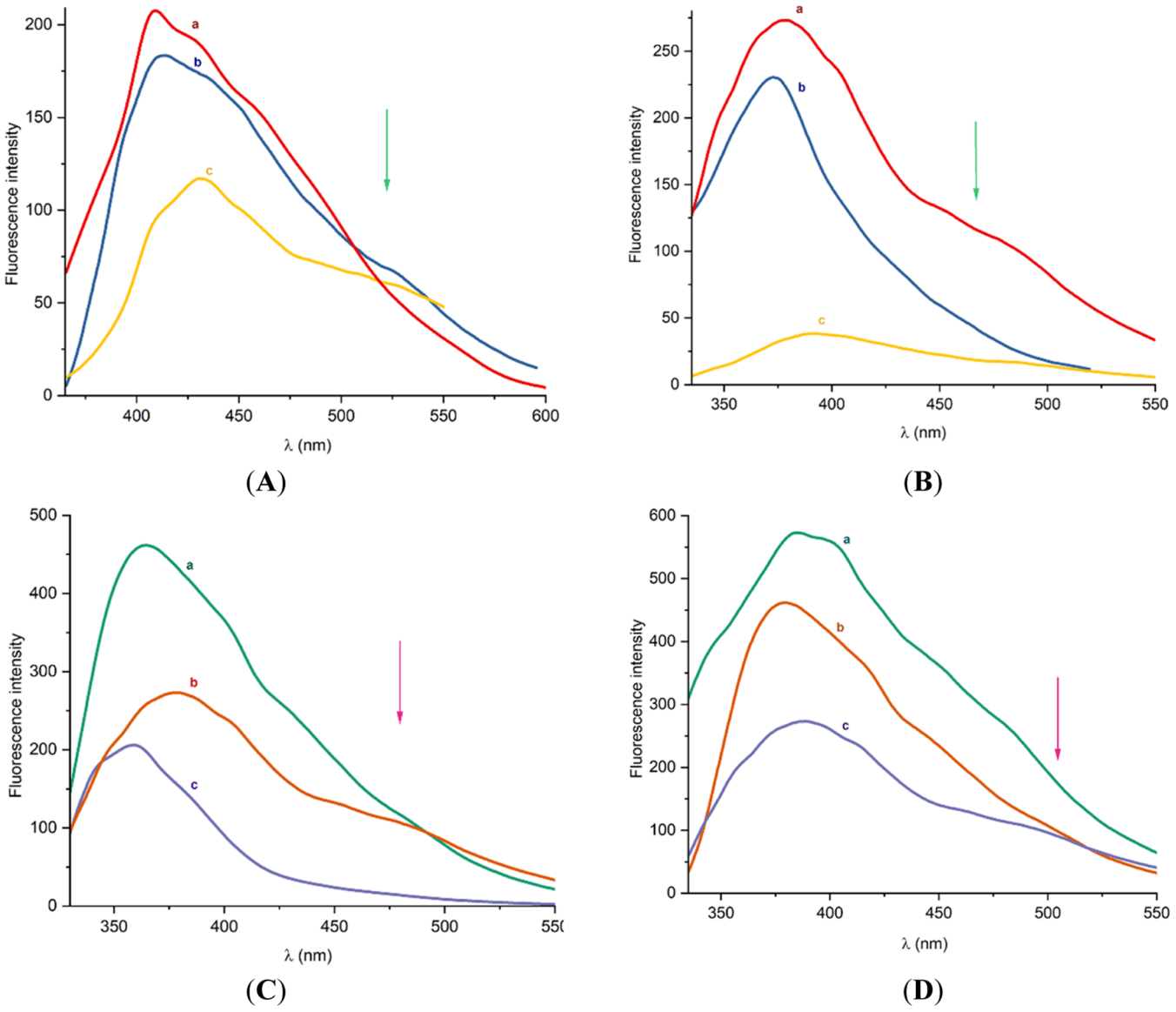

Figure 10. Fluorescence emission spectra of metal nanoparticles for different photoinitiator systems. (A) Fluorescence spectra of AgNPs with BP1 [(a) BP1 0.003 wt % and Ag 2 wt %, (b) BP1 0.003 wt %, Ag 2 wt %, and TEA 1 wt %, (c) BP1 0.003 wt %, Ag 2 wt %, TEA 1 wt %, and Iod 1 wt %]. (B) AgNPs with BP2 [(a) BP2 0.003 wt % and Ag 2 wt %, (b) BP2 0.003 wt %, Ag 2 wt %, and TEA 1 wt %, (c) BP2 0.003 wt %, Ag 2 wt %, TEA 1 wt %, and Iod 1 wt %]. (C) AuNPs with BP1 [(a) BP1 0.003 wt % and Au 2 wt %, (b) BP1 0.003 wt %, Au 2 wt %, and TEA 1 wt %, (c) BP1 0.003 wt %, Au 2 wt %, TEA 1 wt %, and Iod 1 wt %]. (D) AuNPs with BP2 [(a)BP2 0.003 wt % and Au 2 wt %, (b) BP2 0.003 wt %, Au 2 wt %, and TEA 1 wt %, (c) BP2 0.003 wt %, Au 2 wt %, TEA 1 wt %, and Iod 1 wt %].

increasing the size of the nanoparticles. The incident light at 350 nm leads to the excitation of the surface plasmon coherent electronic motion as well as the d electrons.[76] The different sizes of AuNPs and AgNPs (traces a−c) were used to investigate the effect of the size of metal nanoparticles on the fluorescence intensity.

It is observed that the nanoparticle systems show distinctly different emission profiles in the presence of different sizes of gold and silver colloids. The most important feature of physical significance is that the intensity of the emission spectrum increases significantly when progressing from smaller to larger gold and silver particles (traces a−c where the concentrations of the gold and silver are the same) as shown in Figure 10 by traces a−c. Here, a represents the one component system (BP), b represents the bicomponent system, which has the amine (BP/TEA), and c represents the tricomponent system which has amine combine with iodonium salt (BP/TEA/Iod). By changing the size of the nanoparticles, we can notice the interaction of the size and surface effects on the structure of the particles. When the gold and silver concentrations are the same for all sets of particles, the bigger the particle, the lower the concentration of the particles and subsequently the surface area.[77]

4. CONCLUSIONS

This paper discusses new benzophenone derivatives named BP1 and BP2 as photoinitiators utilized originally for the photochemical synthesis of metal nanoparticles under exposure to an LED at 419 nm. The metal nanoparticles were produced by a rapid and efficient method in an organic solvent, by which the silver or gold ions are reduced in the presence of various photoinitiator systems. The NPs generated were controlled in

https://doi.org/10.1021/acsomega.2c06655
ACS Omega 2023, 8, 3207−3220

terms of size, shape, and distribution. The photoinitiator systems used for the formation of metal nanoparticles were BP alone, BP/TEA, and BP/TEA/Iod. To summarize the results of this paper, we can note that the size and distribution of nanoparticles depend on the type of photoinitiator system used. Short irradiation of the mixture containing BP1 and BP2 with gold or silver ions in the presence of triethylamine and iodonium salt was noticed to lead to the formation of nanoparticles with a small size of 4−15 nm, which is considered a good size. After successfully preparing the metal nanoparticles, particles of variable sizes were used to study their effect on the behavior of the emission spectrum intensity. It was found that the fluorescence emission range of the nanoparticles varies with the change, whereas the intensity of the fluorescence emission band increased with the increasing nanoparticle size. In this work, nanoparticles of noble metals were generated, and the ability of the new proposed systems to generate nanoparticles of less expensive precursors will be an interesting perspective.

■ ASSOCIATED CONTENT

Supporting Information

The Supporting Information is available free of charge at https://pubs.acs.org/doi/10.1021/acsomega.2c06655.

Experimental results presented in the Supporting Information include characterization of compound BP2, ^{1}H-NMR spectra of compound BP2, ^{13}C-NMR spectra of compound BP2, cyclic voltammogram response of compounds BP1 and BP2, and emission and excitation spectra of BP1 and BP2 (PDF)

■ AUTHOR INFORMATION

Corresponding Authors

Abrar S. Alnafisah − *Department of Chemistry, College of Science, Qassim University, Buraidah 51452, Saudi Arabia*; Email: alnafisaha@qu.edu.sa

Haja Tar − *Department of Chemistry, College of Science, Qassim University, Buraidah 51452, Saudi Arabia*; orcid.org/0000-0002-9240-9422; Email: H.tar@qu.edu.sa

Authors

Elaf Alqrairy − *Department of Chemistry, College of Science, Qassim University, Buraidah 51452, Saudi Arabia*

Fahad M Alminderej − *Department of Chemistry, College of Science, Qassim University, Buraidah 51452, Saudi Arabia*

Lotfi M. Aroua − *Department of Chemistry, College of Science, Qassim University, Buraidah 51452, Saudi Arabia; Laboratory of Organic Structural Chemistry and Macromolecules, Department of Chemistry, Faculty of Sciences of Tunis, Tunis El-Manar University, 2092 Tunis, Tunisia*

Bernadette Graff − *Institut de Science des Matériaux de Mulhouse IS2M—UMR CNRS 7361—UHA, 68057 Mulhouse, France*

Jacques Lalevee − *Institut de Science des Matériaux de Mulhouse IS2M—UMR CNRS 7361—UHA, 68057 Mulhouse, France*; orcid.org/0000-0001-9297-0335

Complete contact information is available at: https://pubs.acs.org/10.1021/acsomega.2c06655

Notes

The authors declare no competing financial interest.

■ ACKNOWLEDGMENTS

The authors extend their appreciation to the Deputyship for Research& Innovation, Ministry of Education and Qassim University, Saudi Arabia for funding this research work through the project number (QU-IF-5−5−1−32254).

■ REFERENCES

(1) Chu, M.-W.; Myroshnychenko, V.; Chen, C. H.; Deng, J.; Mou, C.; García de Abajo, F. J. Probing bright and dark surface-plasmon modes in individual and coupled noble metal nanoparticles using an electron beam. *Nano Lett.* **2009**, *9*, 399−404.

(2) Lin, S. K.; Cheng, W. T. Fabrication and characterization of colloidal silver nanoparticle via photochemical synthesis. *Mater. Lett.* **2020**, *261*, No. 127077.

(3) Khan, I.; Saeed, K.; Khan, I. Review nanoparticles: properties, applications and toxicities. *Arabian J. Chem.* **2019**, *12*, 908−931.

(4) Kelly, K. L.; Coronado, E.; Zhao, L. L.; Schatz, G. C. The optical properties of metal nanoparticles: the influence of size, shape, and dielectric environment. *J. Phys. Chem. B* **2003**, *107*, 668−677.

(5) Raveendran, P.; Fu, J.; Wallen, S. L. Completely "green" synthesis and stabilization of metal nanoparticles. *J. Am. Chem. Soc.* **2003**, *125*, 13940−13941.

(6) Amirjani, A.; Firouzi, F.; Haghshenas, D. F. Predicting the size of silver nanoparticles from their optical properties. *Plasmonics* **2020**, *15*, 1077−1082.

(7) Lee, K.-S.; El-Sayed, M. A. Gold and Silver Nanoparticles in Sensing and Imaging: Sensitivity of Plasmon Response to Size, Shape, and Metal Composition. *J. Phys. Chem. B* **2006**, *110*, 19220−19225.

(8) Eustis, S.; El-Sayed, M. A. Why gold nanoparticles are more precious than pretty gold: Noble metal surface plasmon resonance and its enhancement of the radiative and nonradiative properties of nanocrystals of different shapes. *Chem. Soc. Rev.* **2006**, *35*, 29−217.

(9) Pitkethly, M. J. Nanomaterials − the driving force. *Mater. Today* **2004**, *7*, 20−29.

(10) Wang, Y.; Xia, Y. Bottom-Up and Top-Down Approaches to the Synthesis of Monodispersed Spherical Colloids of Low Melting-Point Metals. *Nano Lett.* **2004**, *4*, 2047−2050.

(11) Zheng, J.; Zhou, C.; Yu, M.; Liu, J. Different sized luminescent gold nanoparticles. *Nanoscale* **2012**, *4*, 4073−4083.

(12) Ji, X.; Song, X.; Li, J.; Bai, Y.; Yang, W.; Peng, X. Size Control of Gold Nanocrystals in Citrate Reduction: The Third Role of Citrate. *J. Am. Chem. Soc.* **2007**, *129*, 13939−13948.

(13) García-Barrasa, J.; López-de-Luzuriaga, J. M.; Monge, M. Silver nanoparticles: synthesis through chemical methods in solution and biomedical applications. *Cent. Eur. J. Chem.* **2011**, *9*, 7−19.

(14) Elsupikhe, R. F.; Ahmad, M. B.; Shameli, K.; Ibrahim, N. A.; Zainuddin, N. Photochemical Reduction as a Green Method for the Synthesis and Size Control of Silver Nanoparticles in κ-Carrageenan. *IEEE Trans. Nanotechnol.* **2016**, *15*, 209−213.

(15) Jradi, S.; Balan, L.; Zeng, X. H.; Plain, J.; Lougnot, D. J.; Royer, P.; Bachelot, R.; Akil, S.; Soppera, O.; Vidal, L. Spatially controlled synthesis of silver nanoparticles and nanowires by photosensitized reduction. *Nanotechnology* **2010**, *21*, No. 095605.

(16) Sakamoto, M.; Fujistuka, M.; Majima, T. Light as a construction tool of metal nanoparticles: Synthesis and mechanism. *J. Photochem. Photobiol., C* **2009**, *10*, 33−56.

(17) Korchev, A. S.; Bozack, M. J.; Slaten, B. L.; Mills, G. Polymer-Initiated Photogeneration of Silver Nanoparticles in SPEEK/PVA Films: Direct Metal Photopatterning. *J. Am. Chem. Soc.* **2004**, *126*, 10−11.

(18) Batibay, G. S.; Gunkara, O. T.; Ocal, N.; Arsu, N. In-situ photoinduced formation of self−assembled Ag NPs using POSS-TX as nano-photoinitiator in PEGMEA/PEGDA polymer matrix and creating self-wrinkled pattern. *J. Photochem. Photobiol., A* **2018**, *359*, 73−79.

(19) Çeper, T.; Arsu, N. Photochemically Prepared Gold/Polymer Nanocoatings: Formation of Gold Mirror. *Macromol. Chem. Phys.* **2017**, *218*, No. 1700030.
(20) Metin, E.; Batibay, G. S.; Arsu, N. In−situ formation of self-assembled Ag nanoclusters on ct-DNA in the presence of 2-mercaptothioxanthone by using UV−vis light irradiation. *J. Photochem. Photobiol., A* **2018**, *356*, 1−6.
(21) Adibelli, M.; Ozcelik, E.; Batibay, G. S.; Arasoglu, T. O.; Arsu, N. A facile and versatile route for preparation AgNp nanocomposite thin films via thiol-acrylate photopolymerization: Determination of antibacterial activity. *Prog. Org. Coat.* **2020**, *143*, No. 105620.
(22) Tar, H.; Kashar, T. I.; Kouki, N.; Aldawas, R.; Graff, B.; Lalevée, J. Novel Copper Photoredox Catalysts for Polymerization: An In Situ Synthesis of Metal Nanoparticles. *Polymers* **2020**, *12*, No. 2293.
(23) Sangermano, M.; Yagci, Y.; Rizza, G. In Situ Synthesis of Silver−Epoxy Nanocomposites by Photoinduced Electron Transfer and Cationic Polymerization Processes. *Macromolecules* **2007**, *40*, 8827−8829.
(24) Yagci, Y.; Sangermano, M.; Rizza, G. In situ synthesis of gold-cross-linked poly(ethylene glycol) nanocomposites by photoinduced electron transfer and free radical polymerization processes. *Chem. Commun.* **2008**, 2771−2773.
(25) Mallick, K.; Wang, Z. L.; Pal, T. Seed-mediated successive growth of gold particles accomplished by UV irradiation: a photochemical approach for size-controlled synthesis. *J. Photochem. Photobiol., A* **2001**, *140*, 75−80.
(26) Jockusch, S.; Landis, M. S.; Freiermuth, B.; Turro, N. J. Photochemistry and Photophysics of α-Hydroxy Ketones. *Macromolecules* **2001**, *34*, 1619−1626.
(27) McGilvray, K. L.; Decan, M. R.; Wang, D.; Scaiano, J. C. Facile Photochemical Synthesis of Unprotected Aqueous Gold Nanoparticles. *J. Am. Chem. Soc.* **2006**, *128*, 15980−15981.
(28) Marin, M. L.; McGilvray, K. L.; Scaiano, J. C. Photochemical Strategies for the Synthesis of Gold Nanoparticles from Au(III) and Au(I) Using Photoinduced Free Radical Generation. *J. Am. Chem. Soc.* **2008**, *130*, 16572−16584.
(29) Maretti, L.; Billone, P. S.; Liu, Y.; Scaiano, J. C. Facile Photochemical Synthesis and Characterization of Highly Fluorescent Silver Nanoparticles. *J. Am. Chem. Soc.* **2009**, *131*, 13972−13980.
(30) Scaiano, J. C.; Billone, P.; Gonzalez, C. M.; Marett, L.; Marin, M. L.; McGilvray, K. L.; Yuan, N. Photochemical routes to silver and gold nanoparticles. *Pure Appl. Chem.* **2009**, *81*, 635−647.
(31) Stamplecoskie, K. G.; Scaiano, J. C. Light Emitting Diode Irradiation Can Control the Morphology and Optical Properties of Silver Nanoparticles. *J. Am. Chem. Soc.* **2010**, *132*, 1825−1827.
(32) Gonzalez, C. M.; Liu, Y.; Scaiano, J. C. Photochemical Strategies for the Facile Synthesis of Gold−Silver Alloy and Core−Shell Bimetallic Nanoparticles. *J. Phys. Chem. C* **2009**, *113*, 11861−11867.
(33) McGilvray, K. L.; Fasciani, C.; Bueno-Alejo, C. J.; Schwartz-Narbonne, R.; Scaiano, J. C. Photochemical Strategies for the Seed-Mediated Growth of Gold and Gold−Silver Nanoparticles. *Langmuir* **2012**, *28*, 16148−16155.
(34) Pacioni, N. L.; Pardoe, A.; McGilvray, K. L.; Chrétien, M. N.; Scaiano, J. C. Synthesis of copper nanoparticles mediated by photogenerated free radicals: catalytic role of chloride anions. *Photochem. Photobiol. Sci.* **2010**, *9*, 766−774.
(35) Itakura, T.; Torigoe, K.; Esumi, K. Preparation and Characterization of Ultrafine Metal Particles in Ethanol by UV Irradiation Using a Photoinitiator. *Langmuir* **1995**, *11*, 4129−4134.
(36) Esumi, K.; Matsumoto, T.; Seto, Y.; Yoshimura, T. Preparation of gold−, gold/silver−dendrimer nanocomposites in the presence of benzoin in ethanol by UV irradiation. *J. Colloid Interface Sci.* **2005**, *284*, 199−203.
(37) Eustis, S.; Hsu, H.; El-Sayed, M. A. Gold Nanoparticle Formation from Photochemical Reduction of Au3+ by Continuous Excitation in Colloidal Solutions. A Proposed Molecular Mechanism. *J. Phys. Chem. B* **2005**, *109*, 4811−4815.
(38) Eustis, S.; El-Sayed, M. A. Molecular Mechanism of the Photochemical Generation of Gold Nanoparticles in Ethylene Glycol: Support for the Disproportionation Mechanism. *J. Phys. Chem. B* **2006**, *110*, 14014−14019.
(39) Sakamoto, M.; Tachikawa, T.; Fujitsuka, M.; Majima, T. Corrigendum to 'Two-color two-laser fabrication of gold nanoparticles in a PVA film' [Chem. Phys. Lett. 420 (2006) 90−94]. *Chem. Phys. Lett.* **2007**, *442*, No. 170.
(40) Scaiano, J. C. Intermolecular photoreductions of ketones. *J. Photochem.* **1973**, *2*, 81−118.
(41) Turro, N. J.; Ramamurthy, V.; Scaiano, J. C. *Modern Molecular Photochemistry of Organic Molecules*; University Science Books: Sausalito, CA, 2010; pp 219−231.
(42) Kapoor, S. Preparation, Characterization, and Surface Modification of Silver Particles. *Langmuir* **1998**, *14*, 1021−1025.
(43) Eustis, S.; Krylova, G.; Smirnova, N.; Eremenko, A.; Tabor, C.; Huang, W.; El-Sayed, M. A. Using silica films and powders modified with benzophenone to photoreduce silver nanoparticles. *J. Photochem. Photobiol., A* **2006**, *181*, 385−393.
(44) Kapoor, S.; Mukherjee, T. Photochemical formation of copper nanoparticles in poly(N-vinylpyrrolidone). *Chem. Phys. Lett.* **2003**, *370*, 83−87.
(45) Nazar, R. In situ Photosynthesis and Stabilization of Copper Nanoparticles. *Pak. J. Eng. Appl. Sci.* **2017**, *21*, 1−11.
(46) McTiernan, C. D.; Alarcon, E. I.; Hallett-Tapley, G. L.; Murillo-Lopez, J.; Arratia-Perez, R.; Netto-Ferreira, J. C.; Scaiano, J. C. Electron transfer from the benzophenone triplet excited state directs the photochemical synthesis of gold nanoparticles. *Photochem. Photobiol. Sci.* **2014**, *13*, 149−153.
(47) Mirac Dizman, H.; Kazancioglu, E. O.; Shigemune, T.; Takahara, S.; Arsu, N. High sensitivity colorimetric determination of L-cysteine using gold nanoparticles functionalized graphene oxide prepared by photochemical reduction method. *Spectrochim. Acta, Part A* **2022**, *264*, No. 120294.
(48) Eustis, S.; Krylova, G.; Eremenko, A.; Smirnova, N.; Schill, A. W.; El-Sayed, M. Growth and fragmentation of silver nanoparticles in their synthesis with a fs laser and CW light by photo-sensitization with benzophenone. *Photochem. Photobiol. Sci.* **2005**, *4*, 154−159.
(49) Kometani, N.; Doi, H.; Asami, K.; Yonezawa, Y. Laser flash photolysis study of the photochemical formation of colloidal Ag nanoparticles in the presence of benzophenone. *Phys. Chem. Chem. Phys.* **2002**, *4*, 5142−5147.
(50) Scaiano, J. C.; Aliaga, C.; Maguire, S.; Wang, D. Magnetic Field Control of Photoinduced Silver Nanoparticle Formation. *J. Phys. Chem. B* **2006**, *110*, 12856−12859.
(51) Aroua, L. M.; Almuhaylan, H. R.; Alminderej, F. M.; Messaoudi, S.; Chigurupati, S.; Al-mahmoud, S.; Mohammed, H. A. A facile approach synthesis of benzoylaryl benzimidazole as potential α-amylase and α-glucosidase inhibitor with antioxidant activity. *Bioorg. Chem.* **2021**, *114*, No. 105073.
(52) Asadi, M.; Khah, M. S. Some new unsymmetrical diimino tetradentate schiff base derived from 3,4-Diaminobenzophenone: Synthesis, characterization and the formation constant of Ni(II) and Cu(II) complexes. *J. Iran. Chem. Soc.* **2010**, *7*, 875−882.
(53) Rehm, D.; Weller, A. Kinetics of Fluorescence Quenching by Electron and H-Atom Transfer. *Isr. J. Chem.* **1970**, *8*, 259−271.
(54) Huang, T.; Li, Y.; Chen, Y. Benzophenone derivatives as novel organosoluble visible light Type II photoinitiators for UV and LED photoinitiating systems. *J. Polym. Sci.* **2020**, *58*, 2914−2925.
(55) Sharma, Y. R. *Elementary Organic Spectroscopy*, 4th ed.; S. Chand and Company Ltd.: New Delhi, 2010; pp 19−23.
(56) Gencoglu, T.; Graff, B.; Morlet-Savary, F.; Lalevée, J.; Avci, D. Benzophenone-Functionalized Oligo(Amido Amine)/Iodonium Salt Systems as Visible Light Photoinitiators. *ChemistrySelect* **2021**, *6*, 5743−5751.
(57) Karaca Balta, D.; Karahan, Ö.; Avci, D.; Arsu, N. Synthesis, photophysical and photochemical studies of benzophenone based novel monomeric and polymeric photoinitiators. *Prog. Org. Coat.* **2015**, *78*, 200−207.

https://doi.org/10.1021/acsomega.2c06655
ACS Omega 2023, 8, 3207−3220

(58) Liu, S.; Brunel, D.; Sun, K.; Xu, Y.; Morlet-Savary, F.; Graff, B.; Xiao, P.; Dumur, F.; Lalevée, J. A monocomponent bifunctional benzophenone-carbazole type II photoinitiator for LED photoinitiating systems. *Polym. Chem.* **2020**, *11*, 3551−3556.
(59) Rocha, C. S.; Filho, L. F. O. B.; de Souza, A. E.; Diniz, R.; Denadai, Â M. L.; Beraldo, H.; Teixeira, L. R. Structural studies and investigation on the antifungal activity of silver(I) complexes with 5-nitrofuran-derived hydrazones. *Polyhedron* **2019**, *170*, 723−730.
(60) Lalevée, J.; Dumur, F.; Mayer, C. R.; Gigmes, D.; Nasr, G.; Tehfe, M.; Telitel, S.; Morlet-Savary, F.; Graff, B.; Fouassier, J. P. Photopolymerization of N-Vinylcarbazole Using Visible-Light Harvesting Iridium Complexes as Photoinitiators. *Macromolecules* **2012**, *45*, 4134−4141.
(61) Newman, J. D. S.; Blanchard, G. J. Formation of Gold Nanoparticles Using Amine Reducing Agents. *Langmuir* **2006**, *22*, 5882−5887.
(62) Mahmudin, L.; Suharyadi, E.; Utomo, A. B. S.; Abraha, K. Optical Properties of Silver Nanoparticles for Surface Plasmon Resonance (SPR)-Based Biosensor Applications. *J. Mod. Phys.* **2015**, *06*, 1071−1076.
(63) Wiley, B. J.; Im, S. H.; Li, Z.; McLellan, J.; Siekkinen, A.; Xia, Y. Maneuvering the Surface Plasmon Resonance of Silver Nanostructures through Shape-Controlled Synthesis. *J. Phys. Chem. B* **2006**, *110*, 15666−15675.
(64) Burda, C.; Chen, X.; Narayanan, R.; El-Sayed, M. A. Chemistry and Properties of Nanocrystals of Different Shapes. *Chem. Rev.* **2005**, *105*, 1025−1102.
(65) Hartland, G. V. Optical Studies of Dynamics in Noble Metal Nanostructures. *Chem. Rev.* **2011**, *111*, 3858−3887.
(66) Zan, X.; Kozlov, M.; McCarthy, T. J.; Su, Z. Covalently Attached, Silver-Doped Poly(vinyl alcohol) Hydrogel Films on Poly(l-lactic acid). *Biomacromolecules* **2010**, *11*, 1082−1088.
(67) Sakamoto, M.; Tachikawa, T.; Fujitsuka, M.; Majima, T. Acceleration of Laser-Induced Formation of Gold Nanoparticles in a Poly(vinyl alcohol) Film. *Langmuir* **2006**, *22*, 6361−6366.
(68) Mostafavi, M.; Keghouche, N.; Delcourt, M.; Belloni, J. Ultra-slow aggregation process for silver clusters of a few atoms in solution. *Chem. Phys. Lett.* **1990**, *167*, 193−197.
(69) Belloni, J.; Mostafavi, M. *Radiation Chemistry Present Status and Future Trends*; Jonah, C. D.; Rao, B. M., Eds.; Elsevier: Amsterdam, 2001; pp 411−452.
(70) Henglein, A. Physicochemical properties of small metal particles in solution: "microelectrode" reactions, chemisorption, composite metal particles, and the atom-to-metal transition. *J. Phys. Chem. A* **1993**, *97*, 5457−5471.
(71) Foos, E. E.; Snow, A. W.; Twigg, M. E.; Ancona, M. G. Thiol-Terminated Di-, Tri-, and Tetraethylene Oxide Functionalized Gold Nanoparticles: A Water-Soluble, Charge-Neutral Cluster. *Chem. Mater.* **2002**, *14*, 2401−2408.
(72) Fan; Chen, Z.; Brinker, C. J.; Clawson, J.; Alam, T. Synthesis of Organo-Silane Functionalized Nanocrystal Micelles and Their Self-Assembly. *J. Am. Chem. Soc.* **2005**, *127*, 13746−13747.
(73) Matsuda, K.; Ito, Y.; Kanemitsu, Y. Photoluminescence enhancement and quenching of single CdSe/ZnS nanocrystals on metal surfaces dominated by plasmon resonant energy transfer. *Appl. Phys. Lett.* **2008**, *92*, No. 211911.
(74) Lakowicz, J. R. *Principles of Fluorescence Spectroscopy*, 3rd ed.; Springer US: Boston, MA, 2006; pp 277−330.
(75) Dulkeith, E.; Morteani, A. C.; Niedereichholz, T.; Klar, T. A.; Feldman, J.; Levi, S. A.; van Veggel, F. C. J. M.; Reinhoudt, D. N.; Möller, M.; Gittins, D. I. Fluorescence quenching of dye molecules near gold nanoparticles: radiative and nonradiative effects. *Phys. Rev. Lett.* **2002**, *89*, No. 203002.
(76) Abdelhalim, M. A. K.; M Mady, M. Physical Properties of Different Gold Nanoparticles: Ultraviolet-Visible and Fluorescence Measurements. *J. Nanomed. Nanotechnol.* **2012**, *03*, 178−194.
(77) Ghosh, S. K.; Pal, A.; Kundu, S.; Nath, S.; Pal, T. Fluorescence quenching of 1-methylaminopyrene near gold nanoparticles: size regime dependence of the small metallic particles. *Chem. Phys. Lett.* **2004**, *395*, 366−372.

https://doi.org/10.1021/acsomega.2c06655
ACS Omega 2023, 8, 3207−3220